αB-Crystallin is a novel oncoprotein that predicts poor clinical outcome in breast cancer

Jose V. Moyano,[1] Joseph R. Evans,[1] Feng Chen,[1] Meiling Lu,[1] Michael E. Werner,[1] Fruma Yehiely,[1] Leslie K. Diaz,[2] Dmitry Turbin,[3] Gamze Karaca,[4] Elizabeth Wiley,[2] Torsten O. Nielsen,[3] Charles M. Perou,[4] and Vincent L. Cryns[1]

[1]Cell Death Regulation Laboratory, Department of Medicine, Department of Cell and Molecular Biology, and [2]Department of Pathology, Robert H. Lurie Comprehensive Cancer Center, Feinberg School of Medicine, Northwestern University, Chicago, Illinois, USA. [3]Genetic Pathology Evaluation Centre, University of British Columbia, Vancouver, British Columbia, Canada. [4]Department of Genetics and Department of Pathology and Laboratory Medicine, University of North Carolina at Chapel Hill, Chapel Hill, North Carolina, USA.

Recent gene profiling studies have identified a new breast cancer subtype, the basal-like group, which expresses genes characteristic of basal epithelial cells and is associated with poor clinical outcomes. However, the genes responsible for the aggressive behavior observed in this group are largely unknown. Here we report that the small heat shock protein α-basic–crystallin (αB-crystallin) was commonly expressed in basal-like tumors and predicted poor survival in breast cancer patients independently of other prognostic markers. We also demonstrate that overexpression of αB-crystallin transformed immortalized human mammary epithelial cells (MECs). In 3D basement membrane culture, αB-crystallin overexpression induced luminal filling and other neoplastic-like changes in mammary acini, while silencing αB-crystallin by RNA interference inhibited these abnormalities. αB-Crystallin overexpression also induced EGF- and anchorage-independent growth, increased cell migration and invasion, and constitutively activated the MAPK kinase/ERK (MEK/ERK) pathway. Moreover, the transformed phenotype conferred by αB-crystallin was suppressed by MEK inhibitors. In addition, immortalized human MECs overexpressing αB-crystallin formed invasive mammary carcinomas in nude mice that recapitulated aspects of human basal-like breast tumors. Collectively, our results indicate that αB-crystallin is a novel oncoprotein expressed in basal-like breast carcinomas that independently predicts shorter survival. Our data also implicate the MEK/ERK pathway as a potential therapeutic target for these tumors.

Introduction

Breast cancer is the most frequently diagnosed cancer in women and is responsible for 411,000 deaths per year in women worldwide (1). Although clinical indices such as tumor size and grade and axillary lymph node metastases are useful prognostic factors in breast cancer, there is an urgent need to identify molecular characteristics of breast carcinomas that more accurately predict clinical outcome and guide specific therapies for individual patients (2). Recent gene expression profiling of human breast cancer has led to the identification of several subtypes of breast cancer with different clinical outcomes: 2 estrogen receptor–positive (ER-positive) subtypes, a subtype with high expression of the erythroblastic leukemia viral oncogene homolog 2/HER-2 (ErbB2/HER-2) proto-oncogene, a normal breast-like subtype, and a basal-like subtype that expresses genes characteristic of basal epithelial cells and normal breast myoepithelial cells, such as cytokeratin 5 (CK5) and CK17, and does not express ER or ErbB2/HER-2 (3–6). Of these subtypes, the ErbB2/HER-2 and basal-like groups are associated with the shortest overall and relapse-free survival. Unlike the ErbB2/HER-2 subtype, the genes in the basal-like cluster responsible for these cells' clinically aggressive behavior are unknown. Identification of these genes could lead to new targeted therapies for basal-like breast tumors, which account for 15–20% of breast cancer cases.

By exploring existing breast cancer cDNA microarray data (3, 4), we observed that α-*basic–crystallin* (*αB-crystallin*) was commonly expressed in basal-like breast carcinomas and postulated that αB-crystallin might contribute to their aggressive behavior, for several reasons. αB-Crystallin is a member of the small heat shock protein family (which also includes Hsp27), whose members function as stress-induced molecular chaperones to inhibit the aggregation of denatured proteins, thereby promoting cell survival (7). In addition, ectopic expression of αB-crystallin in diverse cell types confers protection against a broad range of apoptotic stimuli, including TNF-α, TNF-related apoptosis-inducing ligand (TRAIL), etoposide, growth factor deprivation, and oxidative stress, while silencing αB-crystallin expression by RNA interference (RNAi) sensitizes cells to apoptosis (8–11). We have previously demonstrated that αB-crystallin inhibits apoptosis by disrupting the proteolytic activation of caspase-3, whereas a pseudophosphorylation mutant αB-crystallin that mimics stress-induced phosphorylation (S19E, S45E, and S59E, abbreviated 3XSE) fails to suppress caspase-3 activation and apoptosis induced by TRAIL or growth factor deprivation (9–11). Others have reported that αB-crystallin binds to the proapoptotic Bcl-2 family members Bax and Bcl-x_S and pre-

Nonstandard abbreviations used: αB-crystallin, α-basic–crystallin; CK, cytokeratin; DCIS, ductal carcinoma in situ; EMT, epithelial-mesenchymal transition; ER, estrogen receptor; ErbB2, erythroblastic leukemia viral oncogene homolog 2; IFBB, immunofluorescence blocking buffer; IHC, immunohistochemistry; MEC, mammary epithelial cell; MEK, MAPK kinase; MTS, 3-(4, 5-dimethylthiazol-2-yl)-5-(3-carboxymethoxyphenyl)-2-(4-sulfophenyl)-2H-tetrazolium; RNAi, RNA interference; RT, room temperature; TBS/T, TBS with 0.1% Tween 20; TMA, tissue microarray.

Conflict of interest: The authors have declared that no conflict of interest exists.

Citation for this article: *J. Clin. Invest.* **116**:261–270 (2006). doi:10.1172/JCI25888.

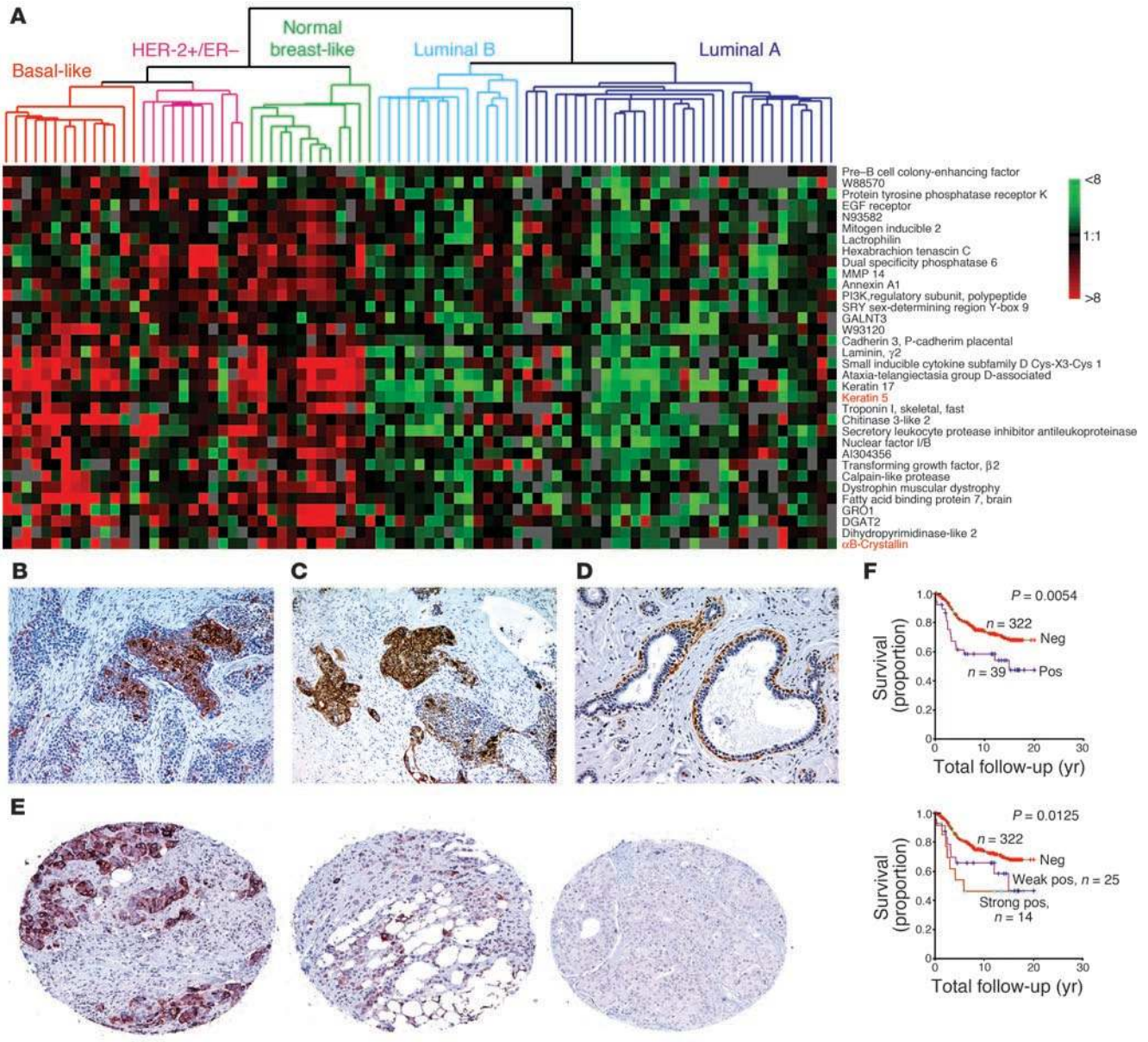

Figure 1

αB-Crystallin is expressed in the basal-like subtype of breast cancer and independently predicts shorter survival. (**A**) Expanded view of the basal epithelial gene expression cluster presented by Sorlie et al. (4) (red, above average gene expression; green, below average gene expression; black, average gene expression). (**B**) αB-Crystallin and (**C**) CK5/6 expression by IHC in the same breast carcinoma that shows a basal-like gene expression and IHC profile. (**D**) Representative immunostaining of normal human breast tissue for αB-crystallin expression. (**E**) αB-Crystallin IHC of 3 representative breast carcinomas in the TMA study: strongly positive (left), weakly positive (middle), and negative (right) examples are shown. (**F**) Kaplan-Meier survival analysis of breast cancer–specific survival based on αB-crystallin expression. Invasive breast carcinomas were scored as positive or negative for αB-crystallin expression (left), or αB-crystallin staining was graded as weakly positive or strongly positive (right). Original magnification, ×100 (**B**–**D**), ×200 (**E**).

vents their translocation to the mitochondria (12). Intriguingly, proteomics analyses revealed that both αB-crystallin and Hsp27 are expressed at greater than 14-fold higher levels in preinvasive ductal carcinoma in situ (DCIS) compared with matched normal breast tissue (13). αB-Crystallin is also expressed in breast cancer and other human cancers, such as gliomas and prostate and renal cell carcinomas (14–16). These findings suggest that the apoptosis resistance conferred by αB-crystallin may contribute to the aggressive behavior of basal-like breast carcinomas.

We report here that αB-crystallin was expressed in approximately half of basal-like breast tumors and predicted shorter patient survival independent of several established prognostic markers. We also show for the first time to our knowledge that overexpression of WT αB-crystallin, but not the pseudophosphorylation mutant, induced neoplastic-like changes in mammary acini grown in 3D culture and transformed immortalized human mammary epithelial cells (MECs). αB-Crystallin overexpression also increased cell migration and invasion in vitro. Strikingly, the transformed

phenotype induced by αB-crystallin was suppressed by inhibitors of the MEK/ERK pathway, which is constitutively activated by αB-crystallin overexpression. Immortalized human MECs overexpressing αB-crystallin formed mammary carcinomas in nude mice that resembled basal-like breast tumors in several respects. Taken together, our results indicate that αB-crystallin is a novel oncoprotein expressed in basal-like breast carcinomas that independently predicts poor clinical outcome. Our data also suggest that inhibition of the MEK/ERK pathway may be an effective therapy for basal-like breast carcinomas expressing αB-crystallin.

Results

αB-Crystallin is expressed in basal-like breast carcinomas and predicts shorter survival. Recent cDNA microarray studies have identified a new breast cancer subtype, termed the basal-like group, which expresses genes characteristic of basal epithelial cells and normal breast myoepithelial cells, such as CK5, and is associated with poor clinical outcomes (3–6). An expanded view of the gene expression data from 115 tumors presented by Sorlie et al. (4) showed that *αB-crystallin* was most consistently expressed in the basal-like tumors and the normal breast samples (Figure 1A). Consistent with these gene expression results, immunohistochemistry (IHC) revealed that αB-crystallin protein was coexpressed with CK5/6 in 2 known basal-like breast tumors (Figure 1, B and C) and was predominantly expressed in myoepithelial cells in normal breast tissue (Figure 1D). We next examined the expression of αB-crystallin by IHC in a tissue microarray (TMA) of invasive breast carcinomas with linked clinical and pathological data (median follow-up, 10.8 yr; range, 0.3–20.0 yr) (17). Tumors were scored as strongly positive (Figure 1E, left), weakly positive (Figure 1E, middle) or negative (Figure 1E, right) for αB-crystallin expression (IHC results for all tumors can be viewed at https://www.gpecimage.ubc.ca/tma/web/viewer.php). αB-Crystallin was expressed in 39 of 361 (11%) breast carcinomas (25 tumors were weakly positive and 14 were strongly positive). Using an IHC surrogate to identify basal-like tumors (negative for ER and ErbB2/HER-2 and positive for EGFR/HER-1 and/or CK5/6) that was validated in an independent breast cancer series (18), we observed that αB-crystallin was expressed in 18 of 40 basal-like breast carcinomas (45%) in the TMA, but only 17 of 288 (6%) nonbasal tumors expressed αB-crystallin ($P = 8 \times 10^{-10}$ by Fisher's exact test). Kaplan-Meier analyses revealed that expression of αB-crystallin in breast carcinomas was associated with shorter disease-specific survival (Figure 1F, left; 10-year disease-specific survival, 59% for αB-crystallin–positive tumors versus 74% for αB-crystallin–negative tumors; $P = 0.0054$). In addition, the levels of expression of αB-crystallin correlated inversely with disease-specific survival: strongly positive tumors were associated with shorter survival than were weakly positive tumors (Figure 1F, right; 10-year disease-specific survival, 46% for strongly positive tumors versus 66% for weakly positive tumors; $P = 0.0125$). In contrast, expression of the related small heat shock protein Hsp27 was not associated with survival in this cohort (ref. 17 and data not shown), thereby underscoring the specificity of our observation. Multivariate Cox regression analysis revealed that αB-crystallin expression predicted shorter survival (hazard ratio, 2.23; $P = 0.001$) independent of tumor grade, lymph node status, and ER and ErbB2/HER-2 expression status (tumor size was not included because accurate measures were unavailable for many cases). These results indicate that αB-crystallin is commonly expressed in basal-like breast carcinomas and is an independent predictor of poor clinical outcome.

Overexpression of αB-crystallin disrupts mammary acini and induces neoplastic abnormalities. In 3D basement membrane culture, human immortalized MECs, such as MCF-10A cells, form acinar-like structures consisting of a single cell layer of polarized, growth-arrested MECs surrounding a hollow lumen (19). Activation of oncogenes such as ErbB2/HER-2 induces neoplastic-like changes in mammary acini, including loss of polarity, increased proliferation, diminished apoptosis, and luminal filling (19, 20). To examine whether overexpression of αB-crystallin induces similar neoplastic abnormalities, we generated by retroviral infection MCF-10A pools that stably expressed either WT αB-crystallin (αB-WT) or a mutant αB-crystallin that mimics stress-induced phosphorylation (αB-3XSE) and is impaired in its antiapoptotic function (10, 11, 21). pLXSN (vector) and parental MCF-10A acini expressed modest levels of αB-crystallin, while the levels in αB-WT and αB-3XSE acini were 11.7-fold and 13.1-fold greater, respectively, than those in parental MCF-10A acini (Figure 2A). Importantly, these levels of αB-WT overexpression are comparable to those observed in DCIS compared with matched normal breast tissue (14.1-fold increase) (13). Although MCF-10A–pLXSN cells formed normal acini similar to those formed by parental cells, MCF-10A–αB-WT cells formed strikingly abnormal acini at a high frequency that were grossly enlarged, disorganized, and hypercellular and contained filled lumens (Figure 2, B and C). Each abnormal αB-WT acinus was formed from a single cell (data not shown). MCF-10A cells stably overexpressing oncogenic H-RasV12 also formed enlarged, disorganized acini with filled lumens (Figure 2B). In contrast, MCF-10A–αB-3XSE cells infrequently formed abnormal acini (Figure 2, B and C). Importantly, αB-WT overexpression also induced similar neoplastic changes in MCF-12A cells (Figure 2B), an immortalized, nontransformed human MEC line unrelated to MCF-10A cells (22). The morphological abnormalities in MCF-10A–αB-WT acini were dependent on αB-crystallin expression: silencing αB-crystallin by retroviral RNAi suppressed the abnormal phenotype of αB-WT acini (Figure 2D). αB-WT (but not αB-3XSE) mammary acini were also characterized by disruption of apicobasal polarity, as determined using GM130 as an apical marker and the integrin β4 subunit and laminin-5 as basolateral markers (Figure 2, E and F). In addition, αB-WT acini had higher expression levels of integrin β4 and laminin-5 than did pLXSN or αB-3XSE acini (Figure 2E and data not shown). αB-WT acini also had diminished luminal apoptosis on day 8, as detected by reduced active caspase-3 immunostaining compared with pLXSN or αB-3XSE acini (Figure 2G, upper panels, and Figure 2H). Furthermore, while pLXSN and αB-3XSE acini underwent proliferative arrest by day 12 as determined by minimal Ki-67 staining, αB-WT acini contained Ki-67–positive cells at day 12 (Figure 2G, lower panels, and Figure 2H). Of note, some αB-3XSE acini exhibited a mild phenotype, characterized by persistence of a few luminal cells at day 12 (Figure 2E, upper panel, and Figure 2G, lower panel). These results indicate that αB-crystallin overexpression in immortalized MECs induces profound abnormalities in acinar architecture that resemble features of preinvasive breast tumors (e.g., DCIS), including enlarged acini with filled lumens, loss of polarity, diminished luminal apoptosis, and increased proliferation (19, 20, 23).

The neoplastic abnormalities in mammary acini overexpressing αB-crystallin are MEK dependent. To identify the mechanisms by which αB-crystallin disrupts mammary acinar architecture, we analyzed MCF-10A pools grown as monolayers in 1% horse serum without added EGF for activation of several key signaling pathways implicated in transformation. We observed that MCF-10A–αB-WT

Figure 2
αB-Crystallin overexpression disrupts mammary acinar morphology. (**A**) Immunoblot of day-12 acini formed by parental MCF-10A cells and MCF-10A pools (pLXSN, αB-WT, and αB-3XSE). αB, αB-crystallin. (**B**) Phase contrast images of day-12 acini formed by parental MCF-10A cells, MCF-10A pools, or an MCF-12A pool stably expressing αB-WT. (**C**) Day-12 acini formed by parental MCF-10A cells or pools were scored for abnormal morphology (enlarged structures with filled lumens), diameter, and cell number per cross section (mid-acini). (**D**) Silencing αB-crystallin in MCF-10A–αB-WT cells by RNAi suppressed the abnormal morphology of αB-WT acini. (**E**) Day-12 pLXSN, αB-WT, or αB-3XSE acini were immunostained with antibodies to αB-crystallin (green) and GM130, an apical marker of polarized epithelium (red, upper panels), or the integrin β4 subunit, a basolateral marker (red, lower panels). Confocal images of mid-acini cross sections are shown. Inset: Higher magnification of the same acinus (magnified ×2.5 of original). (**F**) Percentage of day-12 acini with polarized epithelium. (**G**) pLXSN, αB-WT, and αB-3XSE acini were immunostained with antibodies to αB-crystallin and active caspase-3 (upper panels, day 8) or Ki-67 (lower panels, day 12). (**H**) Percentage of acini that contained ≥2 cells positive for active caspase-3 (day 8) or Ki-67 (day 12). In **A**–**H**, data are mean ± SD ($n = 3$, except RNAi in **D** and laminin-5 polarity in **F**, which were $n = 2$, each in duplicate). *$P < 0.05$ versus control; ***$P < 0.001$ versus pLXSN. Scale bars: 100 μm (**B** and **D**); 50 μm (**E** and **G**).

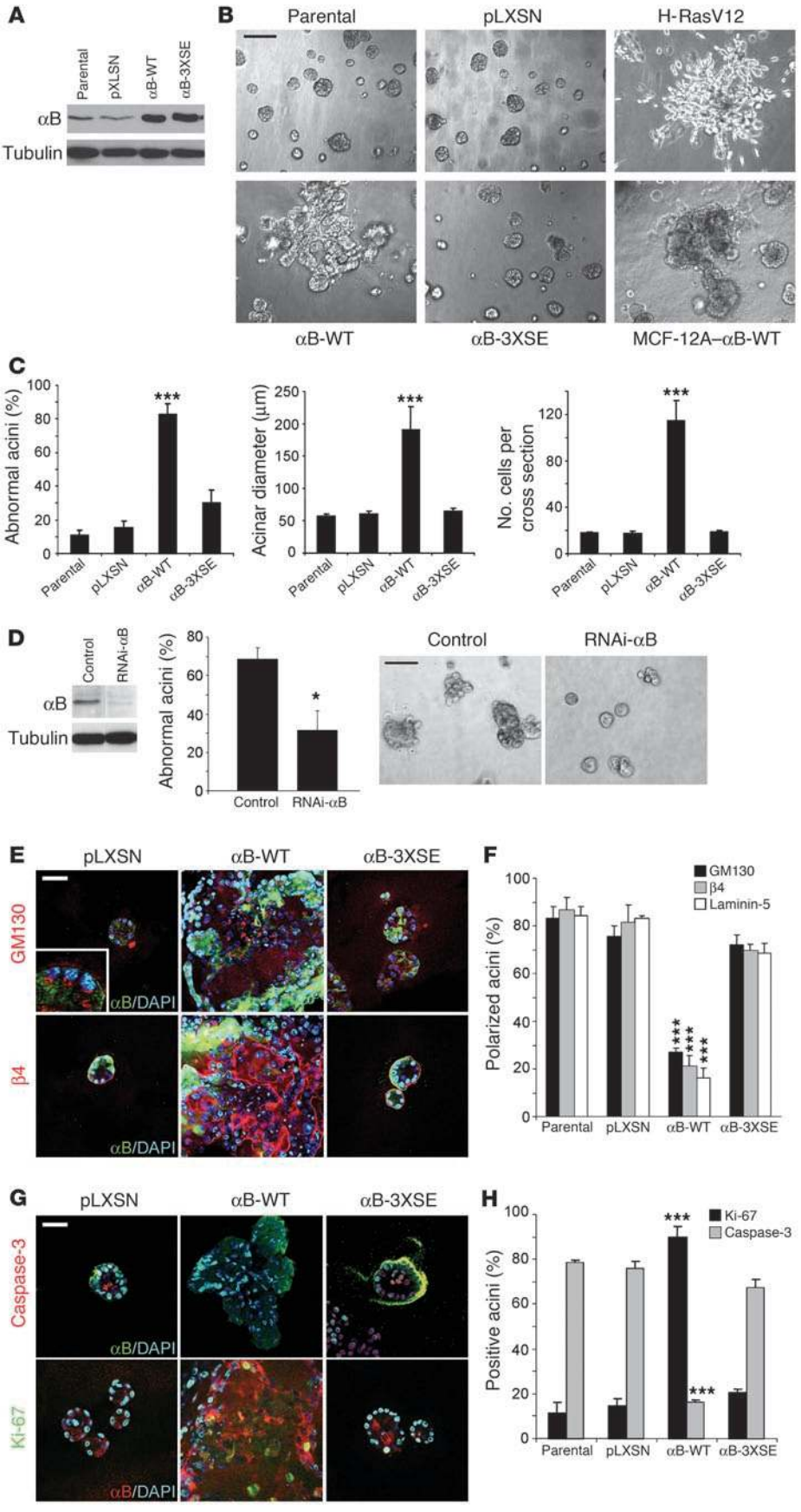

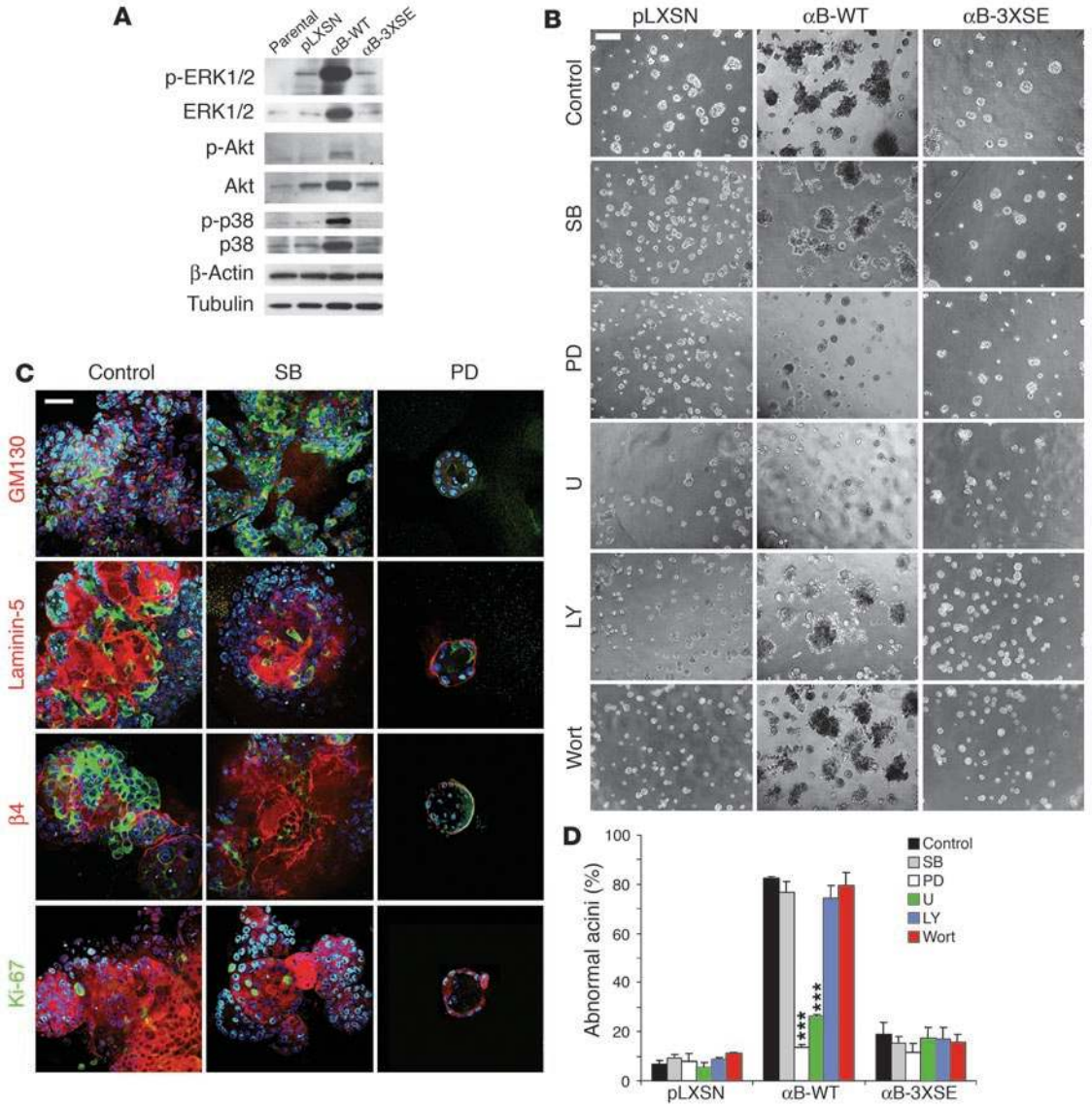

Figure 3

The neoplastic abnormalities in mammary acini overexpressing αB-crystallin are MEK dependent. (**A**) Immunoblot analysis of MCF-10A cells or MCF-10A pools grown as monolayers in low serum without added EGF. p-, phosphorylated. (**B**) MCF-10A pools were plated on Matrigel in the presence of vehicle, 10 μM SB 203580 (SB), 10 μM PD 98059 (PD), 1 μM U 0126 (U), 10 μM LY 294002 (LY), or 0.1 μM wortmannin (Wort). Representative phase contrast images of day-12 acini. (**C**) Representative confocal images of day-12 αB-WT acini cultured from day 0 in the presence of vehicle, SB 203580, or PD 98059 (mid-acini cross sections). Acini were immunostained with antibodies to GM130 (red; αB-crystallin, green), laminin-5 (red; αB-crystallin, green), integrin β4 (red; αB-crystallin, green) or Ki-67 (green; αB-crystallin, red). Nuclei were stained with DAPI (blue). (**D**) Percentage of day-12 acini with abnormal morphology (enlarged structures with filled lumens). MCF-10A pools were treated as in **B**. Data are mean ± SD (n = 3; at least 100 acini scored per experiment). ***P < 0.001 versus control. Scale bars: 100 μm (**B**); 50 μm (**C**).

cells expressed higher levels of total and phosphorylated ERK1/2, Akt, and p38 than did parental MCF-10A, MCF-10A–αB-3XSE, and MCF-10A–pLXSN cells (Figure 3A). MCF-10A pools were then plated on Matrigel in the presence of vehicle (1% DMSO), 10 μM SB 203580, 10 μM PD 98059, 1 μM U 0126, 10 μM LY 294002, or 0.1 μM wortmannin. Although p38 (SB 203580) and PI3K inhibitors (LY 294002 and wortmannin) had no effect on the abnormal morphology of αB-WT acini, αB-WT acini cultured in the presence of the MAPK kinase (MEK) inhibitors PD 98059 and U 0126 were morphologically normal and indistinguishable from pLXSN or αB-3XSE acini (Figure 3, B and D). Moreover, PD 98059, but not SB 203580, restored apicobasal polarity and suppressed proliferation in αB-WT acini (Figure 3C). These results suggest that although αB-crystallin overexpression leads to EGF-independent activation of multiple signaling pathways, selective inhibition of the MEK/ERK pathway is sufficient to inhibit the observed neoplastic abnormalities in αB-WT acini.

Overexpression of αB-crystallin confers EGF- and anchorage-independent growth and MEK-dependent enhanced migration and invasiveness. Because growth factor– and anchorage-independent growth are defining properties of transformed cells (24), we examined whether overexpression of αB-crystallin was sufficient to confer these

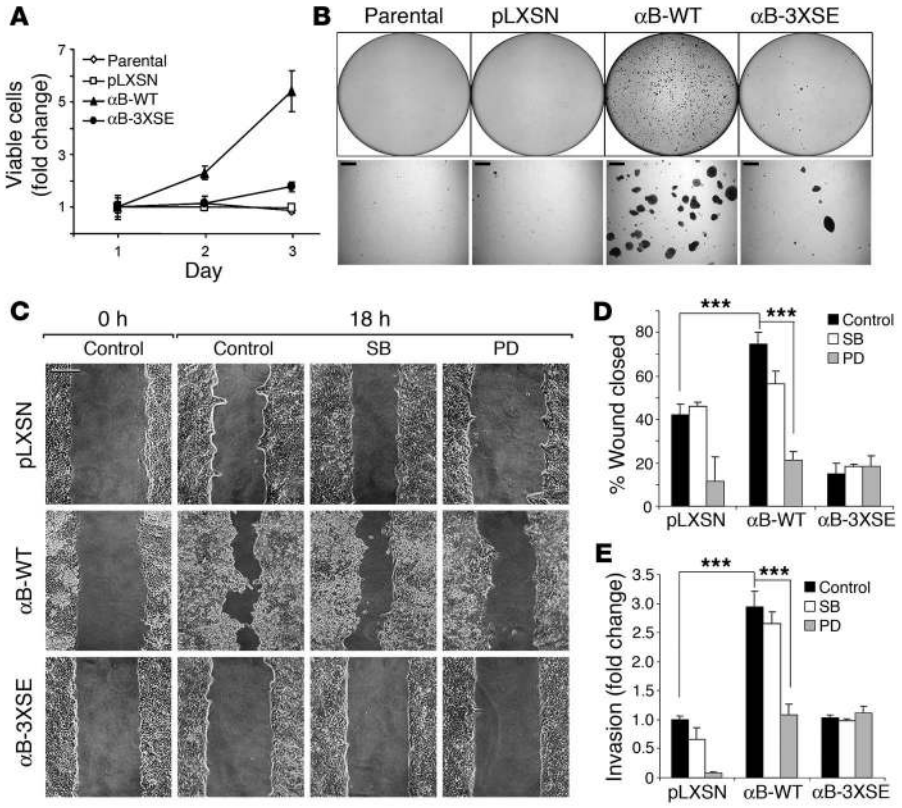

Figure 4
Overexpression of αB-crystallin in MECs confers EGF- and anchorage-independent growth and MEK-dependent enhanced migration and invasiveness. (**A**) Growth of parental MCF-10A cells and MCF-10A pools in low serum (without added EGF) as determined using an MTS viability assay. The results are expressed as fold change in viable cells relative to $t = 0$. (**B**) Representative soft agar colony formation of parental MCF-10A cells and MCF-10A pools: entire well (upper panels) and higher magnification (lower panels). (**C**) Representative micrographs of the wound closure assay of MCF-10A pools treated with vehicle, 10 μM SB 203580 or 10 μM PD 98059 for 18 hours. (**D**) Percentage wound closure. (**E**) MCF-10A pools were placed in a transwell invasion chamber in the presence of vehicle, SB 203580, or PD 98059, and the number of cells invading through Matrigel-occluded pores was determined at 24 hours. The number of invading cells is expressed as fold change from that observed in untreated MCF-10A–pLXSN cells. In **A**–**E**, data are mean ± SD ($n = 3$). ***$P < 0.001$. Scale bars: 500 μm (**B**); 100 μm (**C**).

characteristics on MCF-10A MECs. While parental MCF-10A cells and MCF-10A–pLXSN cells failed to grow in 1% horse serum without added EGF, MCF-10A–αB-WT cells grew rapidly under these conditions, as determined by a 3-(4, 5-dimethylthiazol-2-yl)-5-(3-carboxymethoxyphenyl)-2-(4-sulfophenyl)-2H-tetrazolium (MTS) viability assay (Figure 4A). MCF-10A–αB-3XSE cells exhibited little growth under these conditions. Similar results were obtained through counting cells by trypan blue exclusion (data not shown). Furthermore, MCF-10A–αB-WT cells, but not parental MCF-10A or MCF-10A–pLXSN cells, formed abundant large colonies in soft agar; only rare colonies were observed with MCF-10A–αB-3XSE cells (Figure 4B). These experiments reveal that αB-crystallin overexpression confers EGF- and anchorage-independent growth.

Careful inspection of αB-WT acini revealed that some cells formed protrusions that penetrated the Matrigel (data not shown), suggesting that αB-crystallin overexpression may promote migration and invasion, 2 essential features of malignant tumors (24). To investigate this possibility, we performed cell migration (wound closure) assays. Confluent MCF-10A pools were scraped with a pipette tip and grown for 18 hours in 1% horse serum (without added EGF) supplemented with vehicle, 10 μM SB 203580, or 10 μM PD 98059. Compared with MCF-10A–pLXSN cells, MCF-10A–αB-WT cells exhibited an approximately 2-fold increase in migration, measured as the percentage of the wound closed at 18 hours (Figure 4, C and D). Importantly, trypan blue cell counts at 18 hours revealed nearly identical cell numbers in all groups (cell number at 18 hours was increased only 1.06-fold in αB-WT cells and 1.05-fold in αB-3XSE cells compared with pLXSN cells; data not shown). Hence, the observed differences in wound closure cannot be attributed to differences in cell proliferation. In addition, the migration of MCF-10A–αB-WT cells as well as MCF-10A–pLXSN cells was profoundly inhibited by PD 98059, while SB 203580 had little effect. We next tested the invasiveness of MCF-10A pools using a transwell invasion chamber in which the 8-μm pores were occluded with Matrigel and a gradient of serum was used as the chemoattractant. MCF-10A–αB-WT cells were approximately 3 times more efficient at invading the Matrigel than MCF-10A–pLXSN or MCF-10A–αB-3XSE cells (Figure 4E). MCF-12A cells stably overexpressing αB-crystallin also had increased cell migration and invasion (data not shown). PD 98059, but not SB 203580, inhibited invasion by αB-WT cells and reduced invasion rates in pLXSN, but not αB-3XSE, cells (Figure 4E). These findings indicate that MCF-10A MECs transformed by αB-crystallin overexpression acquire enhanced motility and invasiveness in vitro by a MEK-dependent mechanism.

MCF-10A cells overexpressing αB-crystallin form invasive mammary carcinomas in nude mice. Human MCF-10A MECs are not tumorigenic in nude mice and are a highly stringent model to examine tumorigenicity of oncogenes in vivo (25, 26). To determine whether overexpression of αB-crystallin was sufficient to induce mammary tumors in vivo, we inoculated both mammary fat pads of female athymic nude mice with parental MCF-10A cells or MCF-10A pools (5×10^6 cells in Matrigel) or Matrigel alone. MCF-10A cells were inoculated in a Matrigel suspension to simulate the tumor microenvironment (27). Strikingly, 18 of 20 mammary fat pads inoculated with MCF-10A–αB-WT cells developed tumors (mean volume at 10 weeks, 591 ± 120 mm^3), while only 3 of 20 mammary fat pads inoculated with MCF-10A–αB-3XSE cells developed small tumors (mean volume at 10 weeks, 85.8 ± 27.3 mm^3; $P < 0.01$; Figure 5A). In contrast, none of the mice inoculated with Matrigel alone, parental MCF-10A cells, or MCF-10A–pLXSN cells developed tumors by 13 weeks after inoculation. Small MCF-10A–αB-WT mammary tumors were first palpable 1 week after inoculation and grew pro-

gressively larger throughout the 10-week study, at the end of which some mice were euthanized due to extensive tumor burden. The 3 small MCF-10A–αB-3XSE mammary tumors were first palpable 6 weeks after inoculation and did not grow appreciably (1 tumor completely regressed by week 15; data not shown). Histologic examination of MCF-10A–αB-WT mammary tumors at 5 weeks revealed sheets of elongated mesenchymal-like spindle cells associated with atypical glandular epithelial elements and frank invasion of adjacent muscle and fat, confirming their malignant nature (Figure 5B, upper panels). At week 10, mammary tumors were composed of epithelioid cells with high grade pleomorphic nuclei and abundant mitoses (Figure 5B, lower left panel, thin arrow) that were arranged in glandular-like structures (Figure 5B, lower left panel, thick arrow) and less prominent high nuclear grade spindle cells (Figure 5B, lower right panel). Both 5- and 10-week MCF-10A–αB-WT mammary tumors expressed mesenchymal (vimentin) and epithelial markers (cytokeratins) as well as αB-crystallin (Figure 5C). These findings indicate that overexpression of WT αB-crystallin in MCF-10A cells is sufficient to induce invasive mammary carcinomas in nude mice.

Discussion

We have demonstrated that the small heat shock protein αB-crystallin is a novel oncoprotein: overexpression of WT αB-crystallin was sufficient to transform immortalized human MCF-10A MECs and to induce mammary carcinomas in vivo. Specifically, overexpression of WT αB-crystallin in MCF-10A cells induced profound abnormalities in mammary acini that resembled features of preinvasive tumors: enlarged masses with filled lumens, loss of polarity, increased proliferation, and diminished luminal apoptosis (19, 20, 23). Notably, the abnormal morphology of αB-WT acini was suppressed by silencing αB-crystallin by RNAi. αB-Crystallin overexpression also induced neoplastic changes in immortalized MCF-12A MECs grown in 3D culture, indicating that the observed oncogenic effects are not cell type–specific. Similar neoplastic abnormalities were induced in mammary acini by activating the ErbB2/HER-2 oncogene, which, like αB-crystallin, inhibits apoptosis and promotes proliferation (19, 20). Moreover, overexpression of αB-crystallin in MCF-10A cells induced EGF- and anchorage-independent growth and promoted cell migration and invasion in vitro, which are defining characteristics of malignant neoplasms.

Furthermore, MCF-10A pools stably expressing WT αB-crystallin formed invasive mammary carcinomas in nude mice, thereby confirming the malignant nature in vivo of MCF-10A cells transformed by αB-crystallin. Importantly, the levels of ectopically expressed αB-crystallin observed in mammary acini are comparable to those previously observed in human DCIS (13). In contrast, overexpression of similar levels of a αB-crystallin phosphorylation mutant that mimics stress-induced phosphorylation and is impaired in its cytoprotective function was largely incapable of transforming MECs or initiating mammary tumors, which suggests that the transforming activity of αB-crystallin may be negatively regulated by phosphorylation. These data indicate that αB-crystallin is a bona fide oncoprotein, which to our knowledge was previously unrecognized.

How then does αB-crystallin transform MECs? Although overexpression of αB-WT, but not the 3XSE mutant, induced EGF-independent activation of multiple signaling pathways, the transformed phenotype of MCF-10A–αB-WT cells was selectively suppressed by MEK inhibitors. Indeed, treatment of αB-WT mammary acini with MEK inhibitors restored apicobasal polarity, suppressed proliferation, and promoted apoptosis of centrally located MECs, resulting in morphologically normal acini despite their transformed genotype. These findings are consistent with previously published reports indicating that MEK inhibition suppresses, at least in part, the neoplastic phenotype of breast cancer cells grown in 3D basement membrane culture (28, 29). Constitutively active MEK transforms NIH 3T3 cells, while a dominant-negative MEK

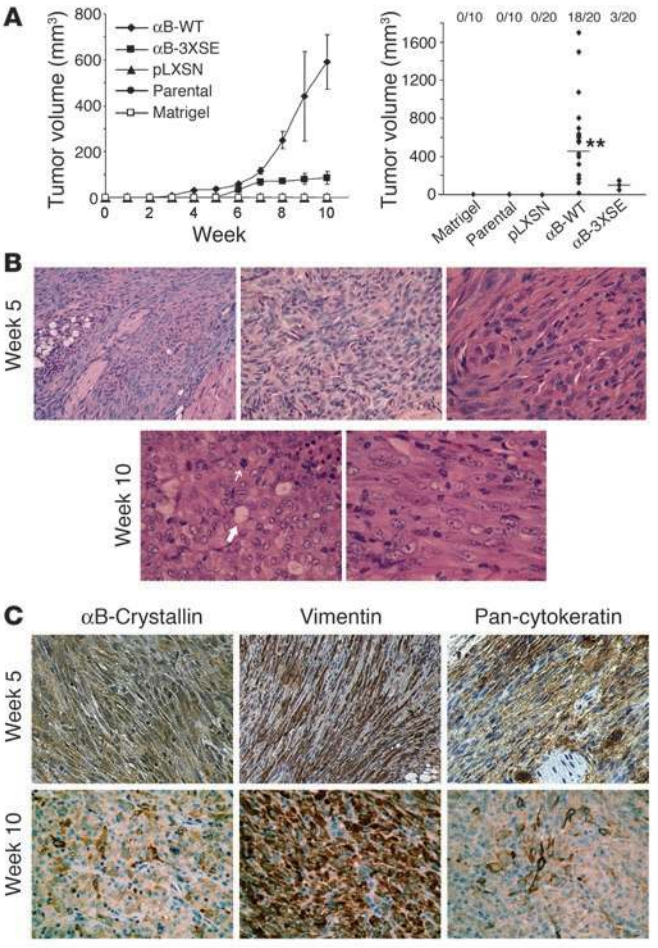

Figure 5

MCF-10A cells overexpressing αB-crystallin form invasive mammary carcinomas in nude mice. (**A**) Left: Mean tumor volume ± SEM at weekly intervals in female athymic nude mice inoculated with MCF-10A pools. Right: Volume of tumors in each group at week 10; horizontal line indicates the median tumor volume in each group. Ratios at top indicate the number of tumors per total inoculation sites. $^{**}P < 0.01$ versus αB-3XSE. (**B**) H&E staining of representative mammary tumors at 5 (upper panels) and 10 weeks (lower panels) from nude mice inoculated with MCF-10A–αB-WT cells. Upper left panel: Prominent elongated spindle cells and atypical epithelial components with tumor invasion of muscle and fat. Upper middle panel: Mesenchymal spindle cells. Upper right panel: Atypical epithelial components. At 10 weeks, we observed epithelioid cells with pleomorphic high grade nuclei and mitoses (thin arrow) that form glandular like structures (thick arrow, lower left panel) and high nuclear grade spindle cells (lower right panel). (**C**) Representative IHC of the mammary carcinomas shown in **B**. Original magnification, ×100 (**B**, upper left panel), ×200 (**B**, remaining panels, and **C**).

inhibitor suppresses transformation by v-Src or H-Ras, indicating a critical role for the Raf/MEK/ERK pathway in transformation (30, 31). Overexpression of αB-crystallin increased levels of total and phosphorylated ERK1/2 protein, a pattern commonly observed in human breast cancer and in MCF-10A cells transformed by H-Ras (32, 33). Although ERK is activated by EGFR/HER family members and integrins in breast cancer (19, 28, 29), our results suggest that αB-crystallin contributes to ERK activation in basal-like tumors. Consistent with this notion, activation of the MEK/ERK pathway produces many of the same consequences we observed by overexpressing αB-crystallin, namely, increased proliferation, reduced apoptosis, and increased cell migration and invasion (34). Clearly, the mechanisms by which αB-crystallin activates ERK have yet to be elucidated. As a molecular chaperone, αB-crystallin may regulate ERK1/2 protein stability and/or phosphorylation/dephosphorylation as Hsp90 regulates Akt and Raf kinase activity (35, 36). Nevertheless, our data indicate unequivocally that the MEK/ERK pathway plays a key role in MEC transformation by αB-crystallin.

We have also demonstrated that MCF-10A–αB-WT cells induced mammary carcinomas in nude mice. In contrast, MCF-10A cells constitutively overexpressing oncogenic H-RasV12, cyclin D1, or ErbB2 do not induce tumors in nude mice, despite promoting anchorage-independent growth in vitro (26, 37, 38), thereby underscoring the tumorigenic potency of αB-crystallin. Early-stage MCF-10A–αB-WT carcinomas had prominent mesenchymal-like spindle cells that expressed αB-crystallin and both mesenchymal (vimentin) and epithelial markers (cytokeratins). These characteristics are strongly suggestive of epithelial-mesenchymal transition (EMT), a process implicated in carcinoma progression, whereby epithelial cells lose polarity and cell-cell adhesion and acquire mesenchymal characteristics such as motility (39). Intriguingly, late-stage carcinomas continued to express αB-crystallin, vimentin, and cytokeratins and retained a less prominent spindle cell component. Although it remains to be determined whether the observed differences in early and late mammary carcinomas represent a temporal progression, it is striking that overexpression of αB-crystallin promoted some aspects of EMT in vitro (disruption of epithelial polarity and enhanced cell migration and invasion) and corresponding histological features in vivo (spindle cells and vimentin expression). Consistent with its potential role in neoplastic EMT, αB-crystallin expression is induced at an early stage during cardiac and skeletal muscle differentiation (mesodermal tissue) and protects myoblasts from apoptosis (10, 40). Both early and late tumors were ER-negative, progesterone receptor–negative (PR-negative), and ErbB2/HER-2–negative (data not shown) and resembled human metaplastic breast carcinomas, a histopathologic subtype notable for mesenchymal spindle cells mixed with epithelial glandular elements (41, 42). Metaplastic carcinomas are also predominantly ER-, PR-, and ErbB2/HER-2–negative and frequently express vimentin and CK5 (43, 44), an expression pattern shared by basal-like breast carcinomas. Hence, the mammary carcinomas induced by αB-crystallin overexpression recapitulated aspects of human basal-like breast tumors, and this xenograft model may be useful for testing new breast cancer therapies. In addition to its role in transformation and tumorigenesis, we recently demonstrated that overexpression of αB-crystallin in breast carcinoma cells promotes their growth as xenograft mammary tumors (11), suggesting that αB-crystallin may also play a role in breast cancer progression.

Although *p53* is commonly mutated in basal-like breast tumors, and *BRCA1* carriers tend to develop these tumors (4, 5), additional genes likely contribute to their aggressive nature. The potent transforming and tumorigenic activity of αB-crystallin, coupled with our observation that αB-crystallin was expressed in approximately half of basal-like breast tumors, suggests that αB-crystallin may contribute to the aggressive behavior of these basal-like tumors. Indeed, we observed that αB-crystallin predicted shorter disease-specific survival independent of tumor grade, lymph node status, and ER and ErbB2/HER-2 status, suggesting that αB-crystallin may provide additional prognostic information for breast cancer patients independent of these established factors. Our findings agree in part with those of a recent study indicating that αB-crystallin expression in breast cancer was associated with lymph node involvement and shorter survival in univariate analyses (14). In contrast to our findings, αB-crystallin expression was not predictive of survival independent of lymph node status in the study by Chelouche-Lev et al. (14). These investigators observed that 88% of breast carcinomas expressed αB-crystallin by IHC, in contrast to the 11% we noted. It is unclear whether these disparities reflect methodological or patient cohort differences. However, our IHC results are consistent with gene expression data from an independent breast cancer cohort indicating that only a minority of breast carcinomas highly express the *αB-crystallin* gene. We are currently examining the expression of αB-crystallin in additional breast cancer cohorts to determine whether αB-crystallin may be a clinically useful predictor of prognosis or drug response. Indeed, the suppression of the transformed phenotype of MCF-10A–αB-crystallin cells by MEK inhibitors in vitro suggest that MEK inhibitors may be an effective therapy for basal-like breast tumors expressing αB-crystallin. Orally active MEK inhibitors have been shown to potently suppress colon cancer growth and melanoma metastasis in xenograft models (45, 46), underscoring the potential feasibility of this therapeutic strategy.

Methods

TMA and IHC analyses. This cohort of 438 patients with invasive breast carcinoma and the corresponding TMA from archival tumor blocks were described previously (17). αB-Crystallin expression was detected by standard IHC methods using a mAb (SPA-222; Stressgen Biotechnologies). Briefly, antigen retrieval was performed by steaming TMA slides in citrate buffer (pH 6.0) for 30 minutes. Endogenous peroxidases were blocked by incubation with 3% hydrogen peroxide for 10 minutes at room temperature (RT). Next, slides were incubated for 30 minutes in Dako protein block at RT and incubated overnight at 4°C with the αB-crystallin mAb (1:200 dilution in Dako antibody dilution buffer). After rinsing in PBS/Tween 20 (0.2%), the slides were incubated with anti-mouse, Dako-labeled polymer for 30 minutes at RT and again rinsed in PBS/Tween 20 (0.2%). Slides were then stained with Nova Red (Vector Laboratories) for 10 minutes at RT, rinsed in distilled water, and counterstained with hematoxylin. αB-Crystallin immunostained tissue core images were digitally captured using a Slide Scanner and WebSlide Browser software (version 3.98; Bacus Laboratories Inc.) as described previously (47). αB-Crystallin immunostaining was scored as strongly positive (≥30% of cancer cells positive), weakly positive (<30% of cancer cells positive), or negative (background level staining only). Statistical analysis was performed in SPSS for Windows (version 11.0; SPSS Inc.). Survival curves were built using the Kaplan-Meier method. *P* values calculated within the Kaplan-Meier method were based on the log-rank test on data pooled over strata. The tumor presented in Figure 1, B and C, was previously described (tumor 97-0137 in ref. 18) and was determined to be basal-like by DNA microarray analyses and IHC studies.

Cell culture and reagents. The immortalized, nontransformed human MCF-10A and MCF-12A MEC lines (22, 25) were purchased from the ATCC.

MCF-10A and MCF-12A cells were cultured in growth medium (DMEM/F12 medium [Invitrogen Corp.] supplemented with 5% horse serum [Invitrogen Corp.], 20 ng/ml EGF [Sigma-Aldrich], 0.5 mg/ml hydrocortisone [Sigma-Aldrich], 100 ng/ml cholera toxin [Sigma-Aldrich], 10 μg/ml insulin [Sigma-Aldrich], and Pen/Strep [Invitrogen Corp.]) as previously described (48). SB 203580, PD 98059, U 0126, LY 294002, and wortmannin were purchased from EMD Biosciences.

Generation of MCF-10A and MCF-12A pools stably overexpressing αB-crystallin. The coding sequences of αB-WT or 3XSE pseudophosphorylation mutant (S19E/S45E/S59E) were PCR amplified from the corresponding plasmids (9, 10) using the following primers: 5′-CCGGGAATTCATGGACATCGCCATCCACC-3′ and 5′-GGCCCTCGAGCTATTTCTTGGGGGCTGCGG-3′. The PCR products were digested with *EcoRI* and *XhoI* and subcloned into the retroviral expression vector pLXSN (BD Biosciences — Clontech). To generate retrovirus, 10 μg plasmid DNA was transfected into the Phoenix amphotrophic retrovirus packaging cell line (ATCC) by standard calcium phosphate methods. We collected media-containing virus 24 hours after transfection, passed it through a 0.45-μm filter, and added 8 μg/mL polybrene. Media was then overlayed on MCF-10A or MCF-12A cells. Forty-eight hours later, pools were generated by selection in 250 μg/mL G418 (Invitrogen Corp.) for 10 days. Stable expression of proteins was confirmed by immunoblotting. For RNAi, pSUPER.retro.puro (OligoEngine)–αB-crystallin was constructed as previously described (11). MCF-10A–αB-WT pools were infected with retrovirus (pSUPER.retro.puro vector or pSUPER.retro.puro–αB-crystallin) and selected in 1 μg/ml puromycin. Silencing of αB-crystallin expression was confirmed by immunoblotting.

3D basement membrane cultures. Twenty-four-well plates precoated with Growth Factor Reduced Matrigel (BD Biosciences) were handled according to the manufacturer's instructions. A single-cell suspension of MCF-10A cells was plated on the Matrigel bed and overlayed with assay medium (DMEM/F12 with 0.5 mg/ml hydrocortisone, 100 ng/ml cholera toxin, 10 μg/ml insulin, and Pen/Strep) supplemented with 2% horse serum, 5 ng/ml EGF, and 2% Matrigel as previously described (48), except that 5×10^3 cells/well were plated on top of the solidified Matrigel. The same protocol was used to grow MCF-12A cells in 3D culture, except they were overlayed with growth medium (described above) and 2% Matrigel. For drug treatments, MCF-10A cells were plated in the presence of vehicle (1% DMSO), 10 μM SB 203580, 10 μM PD 98059, 1 μM U 0126, 10 μM LY 294002, or 0.1 μM wortmannin. Media was changed every 3 days.

3D confocal immunofluorescence. Mammary acini in 24-well plates coated with Matrigel were washed with PBS, fixed with 2% paraformaldehyde for 20 minutes at RT, permeabilized with prechilled 0.5% Triton X-100 for 15 minutes, and washed twice with 100 mM glycine. Matrigel was then gently scraped with a pipette tip and transferred to 2-ml tubes. Matrigel pieces containing acini were centrifuged and blocked with immunofluorescence blocking buffer (IFBB; 7.7 mM NaN_3, 0.1% BSA, 0.2% Triton X-100, 0.005% Tween 20) for 1 hour at RT. Primary antibodies were diluted 1:200 in IFBB, incubated for 2 hours at RT, and washed with IFBB. The following primary antibodies were used: αB-crystallin mAb (SPA-222; Stressgen Biotechnologies), active (large subunit) caspase-3 polyclonal Ab (Cell Signaling Technology), GM130 mAb (BD Biosciences), laminin-5 mAb (Chemicon International), integrin β4 mAb (BD Biosciences), and Ki-67 polyclonal Ab (Zymed). Secondary antibody detection was performed using Alexa Fluor 594 or 488 $F(ab')_2$ fragments of either goat anti-mouse or anti-rabbit IgGs (Invitrogen Corp.) diluted 1:200 in IFBB for 1 hour at RT. Nuclei were stained with 0.5 ng/ml DAPI (Sigma-Aldrich) for 15 minutes at RT. Cells were then washed with IFBB, and the final pellet was resuspended in PBS and mounted on glass slides in Mowiol (Sigma-Aldrich), with DABCO (Sigma-Aldrich) as an antifader. Images were acquired with a Zeiss LSM510 UV META confocal microscope and analyzed with LSM5 software (version 3.1.0; Zeiss).

Western blotting. Matrigel-coated wells containing acini were washed with cold PBS, and 0.4 ml/well of Cell Recovery Solution (BD Biosciences) was added. Immediately, Matrigel was scraped with a pipette tip, and the solution was transferred to 2-ml tubes and placed on ice for 2 hours. Cells were then centrifuged at 500 *g* for 5 minutes at 4°C and washed with cold PBS. Pellets were lysed in RIPA buffer supplemented with 0.1 mM $NaVO_4$ and 0.1 mM NaF. In other experiments, subconfluent monolayers of MCF-10A cells were grown in assay media (described above) supplemented with 1% horse serum (without added EGF) for 18 hours; cell lysates were prepared as described above. Total protein concentration was determined by BCA Protein Assay Kit (Pierce Biotechnology Inc.). Protein (10–20 μg total) was loaded on SDS-PAGE gels and transferred to PVDF membranes (Millipore) using a semidry transfer apparatus (BioRad Laboratories). Membranes were blocked with blocking buffer (5% nonfat milk in TBS with 0.1% Tween 20 [TBS/T]) for 1–2 hours at RT and then incubated with the primary antibody (in TBS/T with 5% BSA) overnight at 4°C. The following primary antibodies were used: αB-crystallin and Hsp27 mAbs (Stressgen Biotechnologies); Akt and phosphorylated Akt mAbs (Ser473), ERK1/2 polyclonal Ab and phosphorylated ERK1/2 (Thr202/Tyr204) rabbit mAb (Cell Signaling Technology); and p38 mAb and phosphorylated p38 (Thr180/Tyr182) polyclonal Ab (BioSource International). After washing with TBS/T, membranes were incubated for 1 hour at RT with the appropriate secondary antibody conjugated to HRP (diluted in TBS/T). Proteins were visualized using the ECL Western Lightning Chemiluminescence kit (PerkinElmer).

Cell growth and soft agar assays. Cells (3×10^3) were seeded in each well of a 96-well plate in phenol-red–free assay medium supplemented with 1% horse serum (without added EGF). The fold change in viable cells on days 1, 2, and 3 compared with day 0 was determined by an MTS assay (CellTiter 96 Aqueous One Solution Cell Proliferation Assay; Promega) as previously described (11). For soft agar assays, 2 ml 0.6% Noble Agar (M-02; Marine BioProducts Inc.) was added to each well of a 6-well plate in growth media (described above) and allowed to solidify. Next, 1 ml/well of a single-cell suspension of 3.3×10^4 MCF-10A cells in growth media containing 0.3% agar was added and allowed to solidify. Growth media (0.5 ml) was added and was replaced every 4 days. Colonies were visualized at 17 days, except parental MCF-10A cells, which were visualized at 21 days.

Cell migration and invasion assays. For cell migration (wound closure) assays, confluent monolayers of MCF-10A cells (6×10^5 cells/well) in 6-well plates were wounded with a 200-μl pipette tip, washed with PBS, and cultured at 37°C in assay medium (described above) supplemented with 1% horse serum (without added EGF). After 18 hours, the wounds were photographed, and the percentage of the wound closed was quantified. For the invasion assays, 2.5×10^4 cells were seeded on top of a Matrigel invasion chamber (8-μm pore diameter; BD Biosciences) in assay medium (described above) supplemented with 1% horse serum (without added EGF); for the lower chamber, assay medium supplemented with 5% horse serum (without added EGF) was used as a chemoattractant. Plates were placed in an incubator at 37°C for 24 hours. Cells invading the lower chamber were stained with 0.5% crystal violet and counted in an inverted microscope.

Mammary tumorigenesis in nude mice. The mammary fat pads of 4- to 5-week-old female athymic nude (nu/nu) mice (Harlan) were inoculated bilaterally with parental MCF-10A cells, MCF-10A pools (5×10^6 cells in 200 μl Matrigel), or Matrigel alone. Tumor volume was measured with Vernier calipers as described previously (11). Tumors were harvested from euthanized mice; formalin-fixed and paraffin-embedded tumor tissue sections were stained with H&E by standard methods. IHC of tumors was performed using mAbs to αB-crystallin (1:200 dilution; Stressgen Biotechnologies), vimentin (clone V9, 1:200 dilution; Sigma-Aldrich) or pan-cytokeratins (AE1/AE3, 1:200 dilution; Dako). All animal procedures were approved by the Animal Care and Use Committee of Northwestern University.

Statistics. The statistical methods for the TMA studies are indicated in "TMA and IHC analysis" in Methods. For all other experiments, the significance of the difference between means was determined by the 2-tailed Student's *t* test for unpaired samples (1-way ANOVA with post-test) using the Instat program (version 3.06; GraphPad Software). A *P* value less than 0.05 was considered significant.

Acknowledgments

We thank Scott W. Lowe for providing the H-RasV12 cDNA. This work was supported in part by NIH grants R01CA097198 (to V.L. Cryns), R01CA10122701 (to C.M. Perou), P50CA89018 (SPORE in Breast Cancer, to V.L. Cryns), P50CA58223 (SPORE in Breast Cancer, to C.M. Perou), T32CA09560 (to J.R. Evans), and T32DK07169 (to M.E. Werner), by Department of Defense Breast Cancer Research Program grants DAMD17-02-1-0526 and DAMD17-03-1-0426 (to V.L. Cryns), and by the Avon Foundation Breast Cancer Research and Care Program (to V.L. Cryns). T.O. Nielsen is a scholar of the Michael Smith Foundation for Health Research.

Received for publication June 8, 2005, and accepted in revised form September 27, 2005.

Address correspondence to: Vincent Cryns, Tarry 15-755, Feinberg School of Medicine, Northwestern University, 303 East Chicago Avenue, Chicago, Illinois 60611, USA. Phone: (312) 503-0644; Fax: (312) 908-9032; E-mail: v-cryns@northwestern.edu.

1. Parkin, D.M., Bray, F., Ferlay, J., and Pisani, P. 2005. Global cancer statistics, 2002. *CA Cancer J. Clin.* **39**:74–108.
2. Gradishar, W.J. 2005. The future of breast cancer: the role of prognostic factors. *Breast Cancer Res. Treat.* **89**:S17–S26.
3. Perou, C.M., et al. 2000. Molecular portraits of human breast tumours. *Nature.* **406**:747–752.
4. Sorlie, T., et al. 2001. Gene expression patterns of breast carcinomas distinguish tumor subclasses with clinical implications. *Proc. Natl. Acad. Sci. U. S. A.* **98**:10869–10874.
5. Sorlie, T., et al. 2003. Repeated observation of breast tumor subtypes in independent gene expression data sets. *Proc. Natl. Acad. Sci. U. S. A.* **100**:8418–8423.
6. Sotiriou, C., et al. 2003. Breast cancer classification and prognosis based on gene expression profiles from a population-based study. *Proc. Natl. Acad. Sci. U. S. A.* **100**:10393–10398.
7. Clark, J.I., and Muchowski, P.J. 2000. Small heat-shock proteins and their potential role in human disease. *Curr. Opin. Struct. Biol.* **10**:52–59.
8. Mehlen, P., et al. 1995. Constitutive expression of human hsp27, Drosophila hsp27, or human αB-crystallin confers resistance to TNF- and oxidative stress-induced cytotoxicity in stably transfected murine L929 fibroblasts. *J. Immunol.* **154**:363–374.
9. Kamradt, M.C., Chen, F., and Cryns, V.L. 2001. The small heat shock protein αB-crystallin negatively regulates cytochrome c- and caspase-8-dependent activation of caspase-3 by inhibiting its autoproteolytic maturation. *J. Biol. Chem.* **276**:16059–16063.
10. Kamradt, M.C., Chen, F., Sam, S., and Cryns, V.L. 2002. The small heat shock protein αB-crystallin negatively regulates apoptosis during myogenic differentiation by inhibiting caspase-3 activation. *J. Biol. Chem.* **277**:38731–38736.
11. Kamradt, M.C., et al. 2005. The small heat shock protein αB-crystallin is a novel inhibitor of tumor necrosis factor-related apoptosis-inducing ligand-induced apoptosis that suppresses the activation of caspase-3. *J. Biol. Chem.* **280**:11059–11066.
12. Mao, Y.W., Liu, J.P., Xiang, H., and Li, D.W. 2004. Human αA- and αB-crystallins bind to Bax and Bcl-X(S) to sequester their translocation during staurosporine-induced apoptosis. *Cell Death Differ.* **11**:512–526.
13. Wulfkuhle, J.D., et al. 2002. Proteomics of human breast ductal carcinoma in situ. *Cancer Res.* **62**:6740–6749.
14. Chelouche-Lev, D., Kluger, H.M., Berger, A.J., Rimm, D.L., and Price, J.E. 2004. αB-Crystallin as a marker of lymph node involvement in breast carcinoma. *Cancer.* **100**:2543–2548.
15. Aoyama, A., et al. 1993. Expression of αB-crystallin in human brain tumors. *Int. J. Cancer.* **55**:760–764.
16. Takashi, M., Katsuno, S., Sakata, T., Ohshima, S., and Kato, K. 1998. Different concentrations of two small stress proteins, αB crystallin and HSP27 in human urological tumor tissues. *Urol. Res.* **26**:395–399.
17. Makretsov, N.A., et al. 2004. Hierarchical clustering analysis of tissue microarray immunostaining data identifies prognostically significant groups of breast carcinoma. *Clin. Cancer Res.* **10**:6143–6151.
18. Nielsen, T.O., et al. 2004. Immunohistochemical and clinical characterization of the basal-like subtype of invasive breast carcinoma. *Clin. Cancer Res.* **10**:5367–5374.
19. Muthuswamy, S.K., Li, D., Lelievre, S., Bissell, M.J., and Brugge, J.S. 2001. ErbB2, but not ErbB1, reinitiates proliferation and induces luminal repopulation in epithelial acini. *Nat. Cell Biol.* **3**:785–792.
20. Debnath, J., et al. 2002. The role of apoptosis in creating and maintaining luminal space within normal and oncogene-expressing mammary acini. *Cell.* **111**:29–40.
21. Ito, H., Okamoto, K., Nakayama, H., Isobe, T., and Kato, K. 1997. Phosphorylation of αB-crystallin in response to various types of stress. *J. Biol. Chem.* **272**:29934–29941.
22. Paine, T.M., Soule, H.D., Pauley, R.J., and Dawson, P.J. 1992. Characterization of epithelial phenotypes in mortal and immortal human breast cells. *Int. J. Cancer.* **50**:463–473.
23. Bissell, M.J., and Radisky, D. 2001. Putting tumours in context. *Nat. Rev. Cancer.* **1**:46–54.
24. Hanahan, D., and Weinberg, R.A. 2000. The hallmarks of cancer. *Cell.* **100**:57–70.
25. Soule, H.D., et al. 1990. Isolation and characterization of a spontaneously immortalized human breast epithelial cell line, MCF-10. *Cancer Res.* **50**:6075–6086.
26. Miller, F.R., Pauley, R.J., and Wang, B. 1996. Activated c-Ha-ras is not sufficient to produce the preneoplastic phenotype of human breast cell line MCF10AT. *Anticancer Res.* **16**:1765–1769.
27. Noel, A., et al. 1993. Enhancement of tumorigenicity of human breast adenocarcinoma cells in nude mice by matrigel and fibroblasts. *Br. J. Cancer.* **68**:909–915.
28. Wang, F., et al. 1998. Reciprocal interactions between β1-integrin and epidermal growth factor receptor in three-dimensional basement membrane breast cultures: a different perspective in epithelial biology. *Proc. Natl. Acad. Sci. U. S. A.* **95**:14821–14826.
29. Wang, F., et al. 2002. Phenotypic reversion or death of cancer cells by altering signaling pathways in three-dimensional contexts. *J. Natl. Cancer Inst.* **94**:1494–1503.
30. Cowley, S., Paterson, H., Kemp, P., and Marshall, C.J. 1994. Activation of MAP kinase kinase is necessary and sufficient for PC12 differentiation and for transformation of NIH 3T3 cells. *Cell.* **77**:841–852.
31. Mansour, S.J., et al. 1994. Transformation of mammalian cells by constitutively active MAP kinase kinase. *Science.* **265**:966–970.
32. Sivaraman, V.S., Wang, H., Nuovo, G.J., and Malbon, C.C. 1997. Hyperexpression of mitogen-activated protein kinase in human breast cancer. *J. Clin. Invest.* **99**:1478–1483.
33. Martinez-Lacaci, I., et al. 2000. RAS transformation causes sustained activation of epidermal growth factor receptor and elevation of mitogen-activated protein kinase in human mammary epithelial cells. *Int. J. Cancer.* **88**:44–52.
34. Sebolt-Leopold, J.S., and Herrera, R. 2004. Targeting the mitogen-activated protein kinase cascade to treat cancer. *Nat. Rev. Cancer.* **4**:937–947.
35. Schulte, T.W., et al. 1996. Destabilization of Raf-1 by geldanamycin leads to disruption of the Raf-1-MEK-mitogen-activated protein kinase signalling pathway. *Mol. Cell. Biol.* **16**:5839–5845.
36. Sato, S., Fujita, N., and Tsuruo, T. 2000. Modulation of Akt kinase activity by binding to Hsp90. *Proc. Natl. Acad. Sci. U. S. A.* **97**:10832–10837.
37. Ciardiello, F., et al. 1992. Additive effects of c-erbB-2, c-Ha-ras, and transforming growth factor-α genes on in vitro transformation of human mammary epithelial cells. *Mol. Carcinog.* **6**:43–52.
38. Zhou, Q., et al. 2000. Cyclin D1 overexpression in a model of human breast premalignancy: preferential stimulation of anchorage-independent but not anchorage-dependent growth is associated with increased cdk2 activity. *Breast Cancer Res. Treat.* **59**:27–39.
39. Thiery, J.P. 2002. Epithelial-mesenchymal transitions in tumour progression. *Nat. Rev. Cancer.* **2**:442–454.
40. Benjamin, I.J., Shelton, J., Garry, D.J., and Richardson, J.A. 1997. Temporospatial expression of the small HSP/αB-crystallin in cardiac and skeletal muscle during mouse development. *Dev. Dyn.* **208**:75–84.
41. Rayson, D., Adjei, A.A., Suman, V.J., Wold, L.E., and Ingle, J.N. 1999. Metaplastic breast cancer: prognosis and response to systemic therapy. *Ann. Oncol.* **10**:413–419.
42. Khan, H.N., et al. 2003. Spindle cell carcinoma of the breast: a case series of a rare histological subtype. *Eur. J. Surg. Oncol.* **29**:600–603.
43. Dunne, B., Lee, A.H., Pinder, S.E., Bell, J.A., and Ellis, I.O. 2003. An immunohistochemical study of metaplastic spindle cell carcinoma, phyllodes tumor and fibromatosis of the breast. *Hum. Pathol.* **34**:1009–1015.
44. Reis-Filho, J.S., et al. 2003. Novel and classic myoepithelial/stem cell markers in metaplastic carcinomas of the breast. *Appl. Immunohistochem. Mol. Morphol.* **11**:1–8.
45. Sebolt-Leopold, J.S., et al. 1999. Blockade of the MAP kinase pathway suppresses growth of colon tumors in vivo. *Nat. Med.* **5**:810–816.
46. Collisson, E.A., De, A., Suzuki, H., Gambhir, S.S., and Kolodney, M.S. 2003. Treatment of metastatic melanoma with an orally available inhibitor of the Ras-Raf-MAPK cascade. *Cancer Res.* **63**:5669–5673.
47. Ng, T.L., et al. 2005. Nuclear β-catenin in mesenchymal tumors. *Mod. Pathol.* **18**:68–74.
48. Debnath, J., Muthuswamy, S.K., and Brugge, J.S. 2003. Morphogenesis and oncogenesis of MCF-10A mammary epithelial acini grown in three-dimensional basement membrane cultures. *Methods.* **30**:256–268.